Article type: Research article

Mechanistic study of coatings relating salt spray performance and molecular build up

Arno Schut[1], Patrick Karpe[1], Damien Cossement[2], Emeline Lachery[2], Sylvain Desprez[2], Mireille Poelman[2]*

1) AXCENTIVE, Chemin de Champouse, FR-13320 BOUC-BEL-AIR, France
2) Materia Nova Research Center, 3 Avenue Nicolas Copernic, Parc Initialis, B-7000 Mons, Belgium

*Correspondance :

Arno Schut, 593 Chemin de Champouse, 13320 Bouc Bel Air, France

E-Mail : a.schut@axcentive.com

Abstract

This paper proposes an innovative approach to characterizing silicon-based chromium(VI) replacement coatings on an Al substrate using, correlatively salt spray tests and time-of-flight secondary ion mass spectrometry (ToF-SIMS) performed in depth profile mode by a gas cluster ion beam source (GCIB). While salt spray tests show the difference in anticorrosion behavior, ToF-SIMS provides molecular information on the entire coating and even down to the interface with the Al substrate. ToF-SIMS revealed $Si_2O_2^+$ and $AlOSi^+$ fragments which both contribute to understanding the differences in the anticorrosion performance found in the salt spray tests. $Si_2O_2^+$ moieties relate to the cross-linking density of the coating and subsequently determine the barrier properties. $AlOSi^+$ originates from the interface and characterizes the actual “” of Al at the interface by the deposited layer. Differences in the depth profile of $Si_2O_2^+$ and $AlOSi^+$ between the 3 samples explained the respective anticorrosion performance. From the tested coatings AC-3 showed the highest intensity for both $Si_2O_2^+$ and $AlOSi^+$ while simultaneously performing the best in the salt spray test. These observations highlight that $Si_2O_2^+$ and $AlOSi^+$ fragments are good indicators of anticorrosion performance and are confirmed by salt spray tests. Moreover AC-3 and AC-2 are true coatings capable of replacing Chromium based systems.

Keywords: silicon-based coatings, chromium replacement, ToF-SIMS depth profile, gas cluster ion beam (GCIB) cross-linking, interface located bond, coatings.

1. Introduction

Within the frame of protecting a metal substrate by corrosion protection coatings, and meeting REACH[1] regulations by avoiding chromium (VI) as a carcinogenic component, silicon-based coatings are nowadays considered as a viable alternative. Sol-gel and preceramic polymers have well evolved from the initial concept of silane monolayers and achieve of the metal interface as well as forming a coating with barrier properties. Initially, it was discovered that silanes could effectively safeguard metals from corrosion. By carefully choosing appropriate silane adhesion promoters, a monolayer of silanes firmly bound to the surface forms a protective film on for example aluminum, titanium and other metals[2,3]. It was later found that sol-gel chemistry provided a better anticorrosive strategy compared to separate silane molecules because it allows for the creation of a more robust and homogeneous coating on the surface of the material. Sol-gel chemistry involves the hydrolysis and condensation of metal alkoxides (f.i. silanes) or metal salts to form a sol, which is a colloidal suspension of nanoparticles in a liquid[4]. The sol-gel can be applied as a coating following standard application methods, such as spray, dip or wiping. When used as a coating, sol-gel chemistry allows for the formation of a uniform, dense, highly crosslinked, and continuous film that is tightly bound to the surface of the substrate. Such film is highly resistant to corrosion and can provide long-lasting protection against environmental factors such as moisture, oxygen, and salt[5]. Furthermore, sol-gel chemistry allows for the incorporation of various functional groups into the coating, which can provide additional benefits such as improved adhesion, durability, and flexibility. Also, the process enables the inclusion of anchoring groups to which subsequent coating layers can adhere, making sol-gels an ideal replacement for chromium-based coatings[6,7].

It is generally accepted that the anticorrosion properties provided by coatings can be measured by salt spray testing and that these coatings rely on the barrier properties and the quality of adhesion to the underlying substrate. However, salt spray testing, while effective, is notoriously time-consuming and expensive and, furthermore, does not distinguish between these two types of characteristics (barrier and adhesion properties) and the way they contribute to anticorrosion properties. This is a real challenge, not the least because the interface bond between the sol-gel and the metal substrate is deeply buried and is expected to be sparse relative to the layer as a whole. However, the ToF-SIMS technique, performed in depth profile mode, is well described in the literature for properly studying these two fundamental aspects[8]. The ToF-SIMS technique allows for obtaining spectra with high detection sensitivity, high mass resolution and molecular information from the targeted material. Abel et al.[9] was the first author to be able to use ToF-SIMS to detect $AlOSi^+$ fragments by gentle etching an assembly of γ-glycidoxypropytrimethoxysilane on oxidized aluminum with a Cs source. The mass accuracy for $AlOSi^+$ was found to be excellent, allowing it to be attributed to interface bonding. Other ToF-SIMS papers highlighted the existence of interface bonds, using either a “direct interface analysis”[10,11] or a depth profile performed with a GCIB source[12]. In the first case, the top silane layer is sufficiently thin (< 5nm) for interface bonding to be easily detected in SIMS spectra, while in the second case the silane layer is very thick (up to 10 µm), which can now be removed by sputtering using current GCIB sources that keep molecular fragments intact, including those occurring at the interface between the coating and the Al substrate.

The aim of this article is to examine three silicon-based coatings (AC-2, AC-3 and AC-1) on an aluminum substrate. These three coatings exhibit different anticorrosion performances which were characterized in parallel by ToF-SIMS and salt spray tests. By the same time, the character of the coatings were evaluated. By correlating ToF-SIMS and salt spray tests, we are proposing an innovative approach which is so far unknown to the best of our knowledge. In addition, this work aims to understand the mechanism of anticorrosion performance.

2. Experimental setup

2.1. Materials

The metal coupons which were used as substrate were cut from aluminum (Al2024, ref. ARX) sheets which were purchased from Q-Panel (thickness of 0.8 mm). Three liquid formulations (AC-2, AC-3 and AC-1) were applied on the Al substrates (see 2.3). The development products were based on silicon based preceramic precursors and differed mainly in organic content. AC-3 is prepared to a complete inorganic polymer, AC-2 contained partly organic components and AC-1 was based on an organic epoxy-based matrix containing inorganic sol-gel based particles.

2.2. Substrate preparation

The aluminum (Al) metal coupons were 1*1 cm^2 pieces which were prepared as follows: i) cleaning by acetone; ii) dipping in NaOH aqueous solution (60g/l) during 10 seconds at 60°C; iii) rinsing by water; iv) dipping in HNO_3 aqueous solution (20%) during 30 seconds at room temperature; v) rinsing by water; vi) drying with dry compressed air.

2.3. Silicon-based coating application

The silicon-based coatings were applied (see 2.1) on Al with the help of a bar coater with a wet thickness of 10 µm. Once the deposition was performed, the metal coupons were cured during one week at room temperature. For the purpose of further characterization of salt spray testing (see 2.4) and ensuring reproducibility, three coated Al coupons were synthesized for each of the 3 formulations. The overall set of replicates for the coated Al coupons were further submitted to salt spray test measurements, except that one coupon was reserved for ToF-SIMS measurements (see 2.5).

2.4. Salt spray test measurements

The coated Al coupons obtained following 2.3 were characterized by neutral salt spray test according to the ISO 7253 normative test (duration of 300 h). The corresponding measurement conditions were: i) NaCl concentration of 5% (+/- 1%); ii) temperature of 35°C (+/-2); iii) use of demineralized water and iv) a pH range between 6.5 – 7.2.

As mentioned in 2.3, the salt spray test measurements were performed for each condition up to 300h, and at intermediate duration times to check the evolution of corrosion as a function of the time.

2.5. ToF-SIMS measurements

ToF-SIMS measurements were conducted with a ToF-SIMS V instrument from ION TOF GmbH (Münster, Germany), used both in depth profile- and surface analytical mode. The instrument is equipped with a pulsed Bi_3^+ liquid metal ion source for analysis and with an Ar gas cluster ion beam (Ar-GCIB) for sputtering (Ar cluster distribution centred on Ar_{1800}^+). Depth profiles were generated in the dual beam mode, consisting of alternating cycles of 30 keV Bi_3^+ analysis for 3.3 seconds followed by a period of 20 keV Ar_{1800}^+ for 33 seconds. During the profile, the Ar_{1800}^+ was operated over a of 450*450 μm^2 area. The Bi_3^+ analysis beam was rastered over 150*150 μm^2 at the center of the sputtering crater. Subsequently the sputtering time abscissa scale could be converted in depth scale. This calculation was conducted by measuring the depth of a sputtering crater, with the help of a stylus mechanical profilometer Dektak 150 from Veeco.

A thorough composition measurement of each coating was further performed by acquiring longer intermediate surface spectra at several location depths within each of the 3 coatings. For this purpose, the depth profile was temporarily paused for acquiring a surface spectrum at the bottom of the freshly obtained sputter crater, for a total duration of 100 seconds.

3. Results and discussion

3.1. Salt spray tests

The results obtained from salt spray tests from AC-2 are shown in Figure 1.

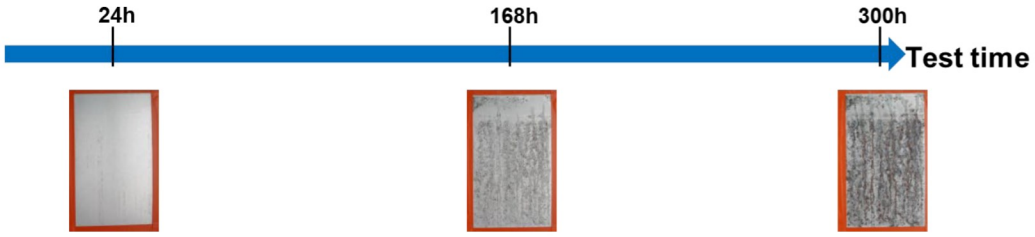

Figure 1. Images of 1 AC-2-coated aluminum coupon after salt spray test measurements for a duration of 24h, 168h and 300h.

After 24h, some corrosion/ pitting (5-10%) can be observed along the direction of the laminate on AC-2. After 168 h, corrosion and pitting had increased to 30-70%. Besides, cracks and corrosion are observed where the coating is thickest. For a total duration of 300h, corrosion is widespread over the entire surface of the coupon.

The results of the AC-3 salt spray tests are shown in Figure 2.

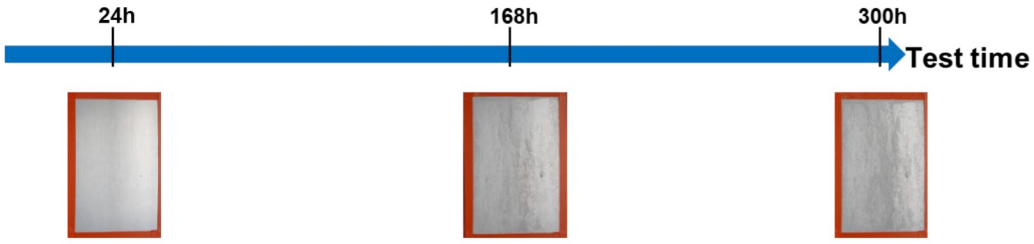

Figure 2. Images of 1 AC-3-coated aluminum coupon after salt spray test measurements for a duration of 24h, 168h and 300h.

After 24 h, a white haze appeared over the entire surface of AC-3, with slight pitting corrosion (~1%). Small defects were also observed on the surface. After 168 hours, white haze and pitting on the surface were in the order of 10-20% respectively. The appearance of a few defects is still observed. For a total duration of 300h, 30% appears to be the maximum range reached for white haze and pitting phenomena, including the appearance of a few defects.

The results of the AC-1 salt spray tests are shown in Figure 3.

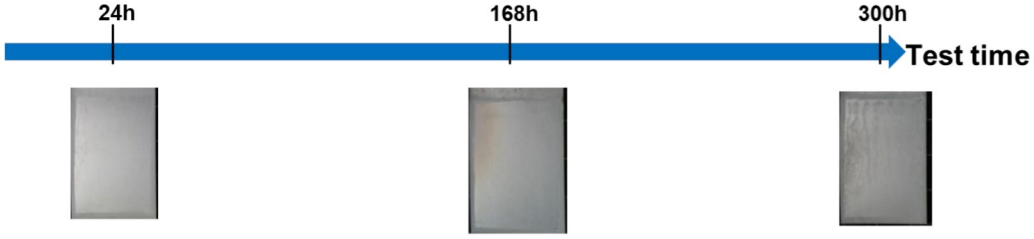

Figure 3. Images of 1 AC-1-coated aluminum coupon after salt spray test measurements for a duration of 24h, 168h and 300h.

After 24 hours, AC-1 shows pitting corrosion over 10-20% of the surface, increasing to 40% and 60% after 168 hours and 300 hours, respectively.

The results presented in Figures 1 to 3 show that AC-3 is the most resistant to corrosion, while AC-2 shows widespread corrosion over the entire surface. AC-1 shows intermediate corrosion resistance compared with AC-2 and AC-3.

3.2. ToF-SIMS

Figure 4 shows the positive ToF-SIMS depth profiles obtained from AC-2, AC-3 and AC-1, from the top surface, through the bulk of the coating and finally to the coating/Al interface. The following ions were extracted: Al^+, Si^+, $AlOH^+$, $AlOSi^+$ and Al_2OH^+. In addition, during the depth profile, the profile was temporarily stopped, so that a long ToF-SIMS surface spectrum was taken at the bottom of the sputter crater, allowing the internal composition of each coating to be measured with improved sensitivity. The dotted vertical lines in Figures 4a-c correspond to the location where a surface spectrum was measured.

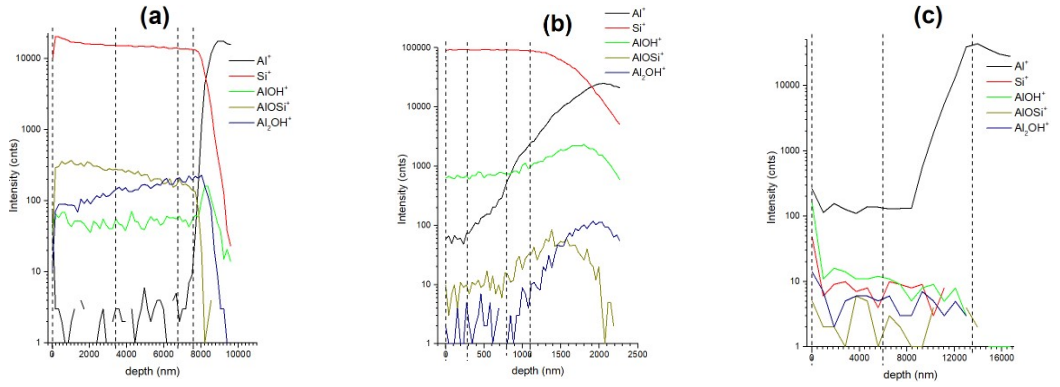

Figure 4. ToF-SIMS depth profile (positive ion mode) obtained from the 3 samples AC-2, AC-3 and AC-1. The following ions were extracted: Al^+, Si^+, $AlOH^+$, $AlOSi^+$ and Al_2OH^+. The vertical dotted lines indicate the depths at which the internal composition of the coating was measured.

In Figure 4, at first glance, a significant difference concerns the overall thickness of each coating, which was estimated at 9.75, 2.3 and 17.65 µm for AC-2, AC-3 and AC-1, respectively. Here, the results are described in terms of composition of the coating, later the layer thickness of the samples will be described.

The profile lines in Figure 4 show broadly the same overall behaviour for all 3 samples, as described below. While Al^+ describes the aluminum substrate, Si^+ defines the coating, and these two profiles taken together confirm that all 3 samples are covered by a coating layer with significant thicknesses, as mentioned above. The Si^+ ion shows a high relative intensity in the case of AC-2 and AC-3 compared to the other ions. However, Si^+ relative to AC-1 appears to be lowest compared to AC-2 and AC-3. This observation indicates that the relative Si content of AC-1 is low.

Beyond these initial observations, the focus is now on the $AlOSi^+$ fragment, which is characteristic of a covalent bond between the substrate and the coating. In the case of AC-2 (Figure 4a), $AlOSi^+$ appears throughout the coating, rather than being specifically localised around the interface. The $AlOSi^+$ for AC-2 suddenly decreases well before the Al^+ line reaches a constant intensity characteristic of the Al substrate. This can be explained by considering the $AlOH^+$ line in parallel with $AlOSi^+$. As the Al substrate is very rough, the $AlOH^+$ line, characteristic of the hydrated Al surface, appears constant throughout the coating, before reaching a peak at the Al coating/substrate. At this point, it can be understood that the inherent roughness of the substrate makes the $AlOH^+$ ion detectable throughout the coating. The observation of the $AlOH^+$ ion may explain the trend observed for the $AlOSi^+$ ion, if we consider that some of the AlOH groups are converted to AlOSi ions, with the result that $AlOH^+$ and $AlOSi^+$ ions coexist in the coating part of the profile, both with significant relative intensities, these findings are consistent with previous literature data[9]. The occurrence of $AlOSi^+$ throughout the thickness of the overall coating (9.75 µm for AC-2) is in agreement with the general definition of a coating of the silicon-based reagent with the Al metal.[13]

Before continuing with the description of the $AlOSi^+$ fragment (theoretical m/z = 70.9534), we considered Al_2OH^+ (theoretical m/z = 70.965), as these two fragments are close to each other in the mass spectra. Firstly, the mass resolution required to separate these two fragments is calculated at 5900, and the experimental value measured for $AlOSi^+$ was 7500, which confirms the good discrimination of these two fragments as described in previous studies [9]. Secondly, we need to check whether $AlOSi^+$ and Al_2OH^+ describe specific and related trends. If we look at the Al_2OH^+ line in Figure 4a, this occurs throughout the coating, in the same way as described for $AlOH^+$ characteristic of the rough, hydrated Al surface. The notable difference between the intensity of $AlOSi^+$ and Al_2OH^+ is that the former falls parallel to Si^+ and, moreover, well before the Al^+ ion has reached the constant intensity characteristic of the bulk of the Al substrate. As for the intensity of Al_2OH^+, it decreases until it becomes zero at the same time as that of $AlOH^+$. Taken together, these observations mean that $AlOSi^+$, even though it occurs at an m/z close to that of Al_2OH^+, describes a specific trend in line with the interface binding expected for AC-2.

Regarding the $AlOSi^+$ fragment for AC-3 (Figure 4b), the relative intensity is low and quite noisy down to 720 nm and simultaneously in this depth region, the Al_2OH^+ intensity is barely detectable, i.e., as low as in the background range. This indicates that hydrated aluminum oxide reacts more efficiently with the coating reagent to form AC-3 than AC-2. At depths greater than ~720 nm, $AlOSi^+$ for AC-3 increases to reach a maximum at ~1400 nm, and finally falls down to zero at 2060 nm. Therefore, the significant thickness, over which the $AlOSi^+$ line extends, indicates that AC-3 meets the definition of a coating. The depth at maximum for $AlOSi^+$ is well before the maximum relative intensity of the peak region shown by $AlOH^+$ and Al_2OH^+, both of which describe the hydrated top layer on the aluminum substrate. The direct difference between AC-2 and AC-3 is that the $AlOSi^+$ moiety in the former is distributed throughout the whole coating, whereas in the latter it shows a more localised peak around the coating/aluminum substrate interface.

Examination of the $AlOSi^+$ fragment for AC-1 (Figure 4c) proved irrelevant in the profile. Indeed, the Si^+ fragment in this case is barely perceptible in the background intensity range, unlike the case of AC-2 and AC-3, for which Si^+ was described as the most intense ion characteristic of the corresponding coating (Figure 4a and 4b). Careful study of the profile line of the $AlOSi^+$ fragment for AC-1 revealed zero intensity for this fragment.

To elucidate the non-detection of the $AlOSi^+$ fragment in the case of AC-1, we studied this fragment throughout the coating up to the coating/Al substrate interface, and compared these data with the internal composition of the other 2 coatings (AC-2 and AC-3). The corresponding positive ToF-SIMS spectra (long acquisition time) are shown in Figure 5.

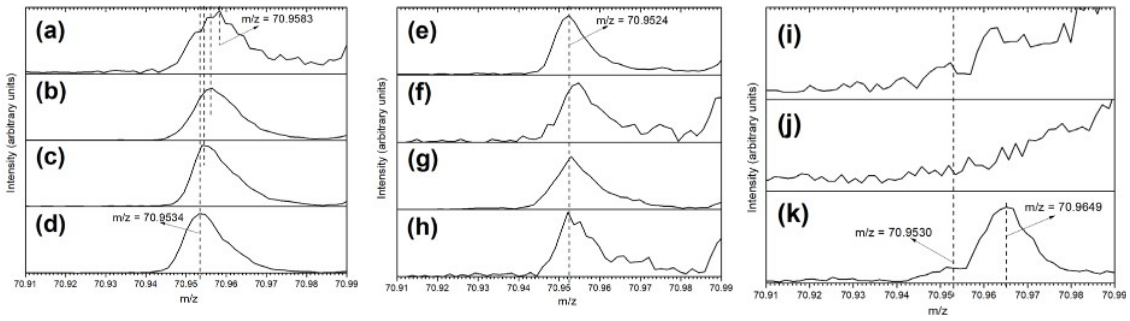

Figure 5. ToF-SIMS spectra (positive ions, m/z between 70.91 and 70.99) recorded for AC-2 at (a) the surface and at the bottom of the sputter crater while having paused the profile and at depths of (b) 3.4 µm, (c) 6.8 µm and (d) 7.6 µm (= coating/ Al substrate interface). Are also added the corresponding data for AC-3 at (e) the surface and at depths of (f) 0.3 µm, (g) 0.8 µm and (h) 1.1 µm (= coating/ Al substrate interface), and for AC-1 at (i) the surface and at depths of (j) 4.9 µm and (k) 12.7 µm (= coating/ Al substrate interface).

Figures 5a-d show a progressive change in peak position from m/z = 70.9583 to a minimum of 70.9534, the former being close to the theoretical m/z ratio of Al_2OH^+ (70.9658), while the latter corresponds precisely to the $AlOSi^+$ fragment (theoretical m/z = 70.9534). This observation means that depth profiling in the coating is accompanied by a slow change in composition in this m/z region, from hydrated aluminum oxide (around the surface region) to Al-O-Si bonds (around the coating/aluminum substrate interface).

In the case of AC-3 (Figures 5e-h), the situation is quite different, as the peak detected in this m/z region is indeed constant at 70.9524, which is close to the theoretical m/z ratio for $AlOSi^+$ (70.9534). This observation is consistent with the description in Figure 2b which indicates a higher reaction yield of Al_2OH^+ to $AlOSi^+$ for AC-3, from the surface to the bulk of AC-3, compared to AC-2.

Examining Figures 5i-j for AC-1, the top surface as well as most of the corresponding coating show no detection of Al_2OH^+ and $AlOSi^+$, meaning that the hydrated aluminum oxide surface is well covered by the coating which contains little Si, as explained in Figure 4c. Consequently, no $AlOSi^+$ fragments could be detected to reveal the coating/substrate interface. However, running the surface spectrum around the interface region for AC-1 (Figure 5k) revealed $AlOSi^+$ at m/z = 70.9530, in close proximity to Al_2OH^+ noticed at m/z = 70.9649. This result confirms that AC-1 exhibits an Al-O-Si interface bond, like AC-2 and AC-3, but with a very low relative intensity. This result suggests that the density of interface bonds between the coating and the underlying substrate is the lowest, when considering samples AC-2 and AC-3.

In addition to the $AlOSi^+$ fragment, another interesting m/z range (between m/z = 115.00 and 115.10) of positive spectra was found to confirm the results described above (Figure 6).

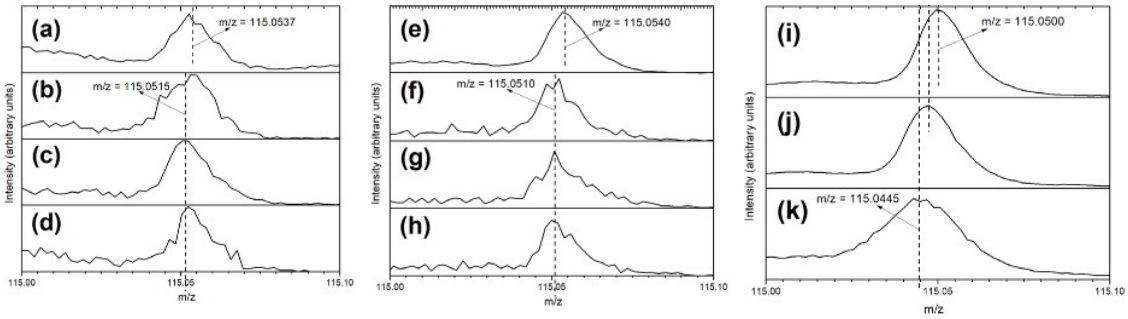

Figure 6. ToF-SIMS spectra (positive ions, m/z between 115.00 and 115.10) recorded for AC-2 at (a) the surface and at the bottom of the sputter crater while having paused the profile at depths of (b) 3.4 µm, (c) 6.8 µm and (d) 7.6 µm (= coating/ Al substrate interface). Are also added the corresponding data for AC-3 at (e) the surface and at depths of (f) 0.3 µm, (g) 0.8 µm and (h) 1.1 µm (= coating/ Al substrate interface), and for AC-1 at (i) the surface and at depths of (j) 4.9 µm and (k) 12.7 µm (= coating/ Al substrate interface).

Samples AC-2, AC-3 and AC-1 all show, in the upper region of the surface (Figures 6a, 6e and 6i), the $C_9H_7^+$ fragment (m/z theoretical = 115.048) that is frequently encountered in ToF-SIMS surface analyses[14]. This can be explained by adventitious surface hydrocarbon contamination which builds up at the surface, following contact of surface sample with the ambient atmosphere.

After the surface, the depth composition of AC-2 (Figures 6b-d) and AC-3 (Figures 6f-h) shows a peak in this region that is displaced from $C_9H_7^+$ (theoretical m/z = 115.0548) to m/z = 115.0515 (AC-2) and 115.0510 (AC-3). The chemistry of this peak can be attributed to $SiH_{11}N_2O_3^+$ = 115.039). Although this chemical attribution is the most likely, it cannot be firmly confirmed at this stage, given that synthesis of the products has not been followed by chemical analysis and thus the exact reaction products and byproducts could not be confirmed. the exact composition of the reagents used to synthesise the coatings is not known. In addition, the consistent occurrence of these fragments for AC-2 and AC-3 is worth mentioning as it may contribute to the anticorrosion properties of the corresponding coatings.

In the case of AC-1, a similar shift can be observed, but with a significantly lower magnitude (see m/z = 115.0500 for $C_9H_7^+$ at 115.0445) than that observed for AC-2 and AC-3. A likely explanation lies in the high hydrocarbon content of AC-1, which gives rise to a high relative intensity of $C_9H_7^+$ that may overshadow the silicon-containing peak observed at m/z = 115.0510 for AC-2 and AC-3. In addition, this fragment may be barely detectable due to the low Si content observed for AC-1.

Figure 7 shows the positive ToF-SIMS depth profiles obtained for AC-2, AC-3 and AC-1. Particular emphasis is placed on drawing, in addition to Al^+ and Si^+, the $Si_2O_2^+$ fragment because it represents the cross-linked silica parts of the sol-gel.

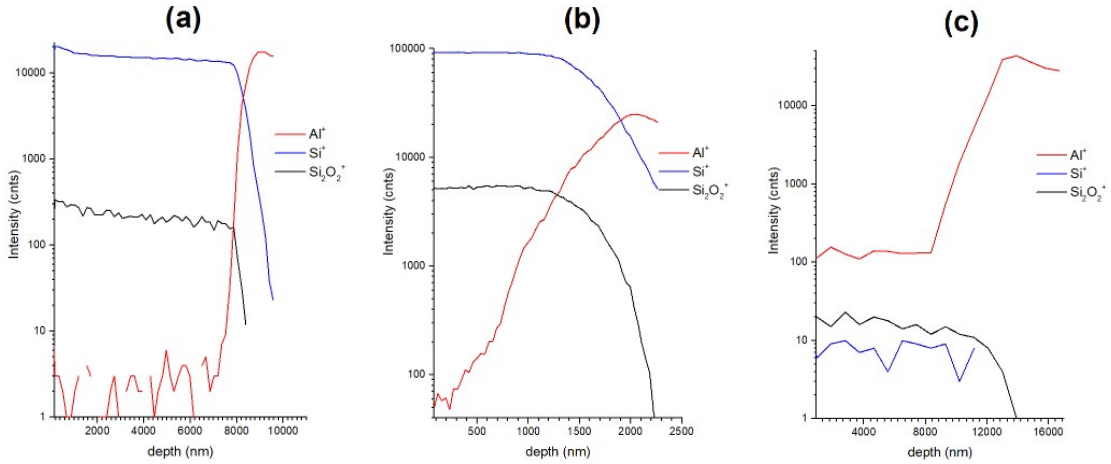

Figure 7. ToF-SIMS depth profile (positive ion mode) obtained from the 3 samples AC-2, AC-3 and AC-1. The following ions drawn are Al^+, Si^+ and $Si_2O_2^+$.

Figure 7 shows for the 3 samples that the $Si_2O_2^+$ fragment, which is characteristic of the cross-linked parts in the coating, displays a high relative intensity and follows the Si^+ line. This observation confirms the high crosslink density of the coatings for AC-2, AC-3 and AC-1.

Figure 8 shows the negative ToF-SIMS depth profiles obtained from AC-2, AC-3 and AC-1, with particular emphasis on the CN^- and AlO_2^- lines. The 3 profiles show that the 3 coatings all contain nitrogen thanks to the detection of CN^-. In addition, for AC-2 and AC-1, the AlO_2^- line, which corresponds to the detection of aluminum oxide, is detected in the bulk of these 2 coatings at a background level, whereas AC-3 shows no significant detection of the AlO_2^- line in the bulk of the coating, which increases sharply from ~ 1200 nm and thus defines the substrate. This observation is in line with the previous finding in Figure 5 where the highest reaction yield of surface aluminum hydroxide to $AlOSi^+$ was detected for AC-3.

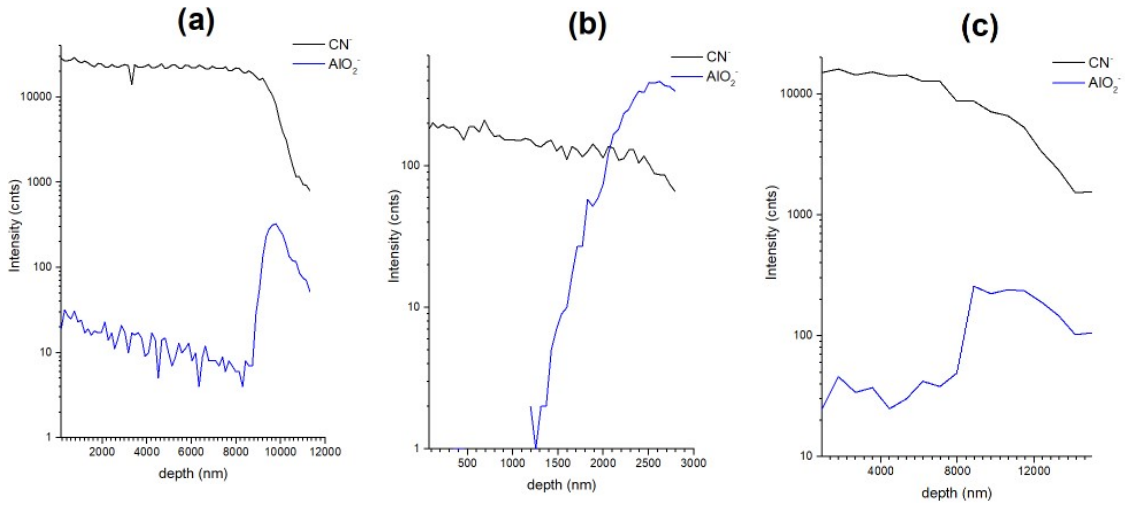

Figure 8. ToF-SIMS depth profile (negative ion mode) obtained from the 3 samples AC-2, AC-3 and AC-1. The following ions are CN^- and AlO_2^-.

3.3. Correlation between ToF-SIMS and salt spray test results

By correlating ToF-SIMS analysis with the actual salt spray test results, we can now explain and predict the corrosion resistance properties of coatings with the help of the analytical features of ToF-SIMS. As previously reported in the literature[15], two main factors are known to govern corrosion resistance, namely the interface bond between the coating and the substrate, and the degree of cross-linking of the coating both defined by the chemical nature of the silicon-based coatings. Beyond these characteristics, the “” character of the coatings is another property to consider. A fourth physical factor which may not be neglected is the thickness of the coating, as this can modulate the barrier properties of the coating. These four factors are examined in turn.

From the salt spray tests it can be concluded within the 300 hrs time frame that AC-3 is much more resistant to corrosion than AC-2, subject to widespread corrosion after 168 hrs of salt spray. AC-1 is in an intermediate position compared with the previous two.

When examining the interface bonding between the silicon-based coating and the substrate (Figure 9a), the $AlOSi^+$ profile line for AC-3 is more localised around the Al coating/substrate interface than in the case of AC-2, which occurs throughout the interior of the coating. The $AlOSi^+$ profile line for AC-1 was not detected, even though interface binding was confirmed when longer surface spectra were run in the interface region. As the $AlOSi^+$ extends over a significant depth for AC-3 (several hundreds of nm) as well as for AC-2 (approximates 10 µm), these two samples can be qualified as “” coatings,whereas AC-1 should be seen as an effective organic barrier coating. In addition, the AlO_2^- profile line (Figure 8) showed zero intensity in the coating for AC-3, while a background intensity was noted in the case of AC-2, suggesting a high yield reaction of the surface aluminum hydroxide with the coating reagent to $AlOSi^+$ in the case of AC-3. It can be concluded that the specific location of the $AlOSi^+$ profile line close to the aluminum surface proves to be a significant factor in the high corrosion resistance performance. The specific fragment identified as $SiH_{11}N_2O_3^+$ (Figure 6) at m/z = 115.0510 -115.

0515 seen both in AC-3 and AC-2 is probably not the most important factor in the corrosion resistance as it is not significantly different between AC-3 and AC-2 (see $SiH_{11}N_2O_3^+$ profile line in Figures 9a and 9b). The $C_9H_7^+$ moiety close to $SiH_{11}N_2O_3^+$ shows a high relative intensity for AC-1 (Figure 9c) can be attributed to the high organic content of this coating and may contribute to the barrier properties of the corresponding coating, perhaps through the hydrophobic character given by the AC-1 coating.

Next to the formation of the $AlOSi^+$ moieties, the efficiency of the silicon-based coating can be constructed by the formation of polymeric silica revealed by $Si_2O_2^+$ elements (Figure 9c). Clearly AC-3 shows the highest relative intensity for this ion, AC-2 is in between, while AC-1, in contrast, shows the lowest relative intensity, which was already observed by the low relative intensity of Si^+ described above (Figure 4c).

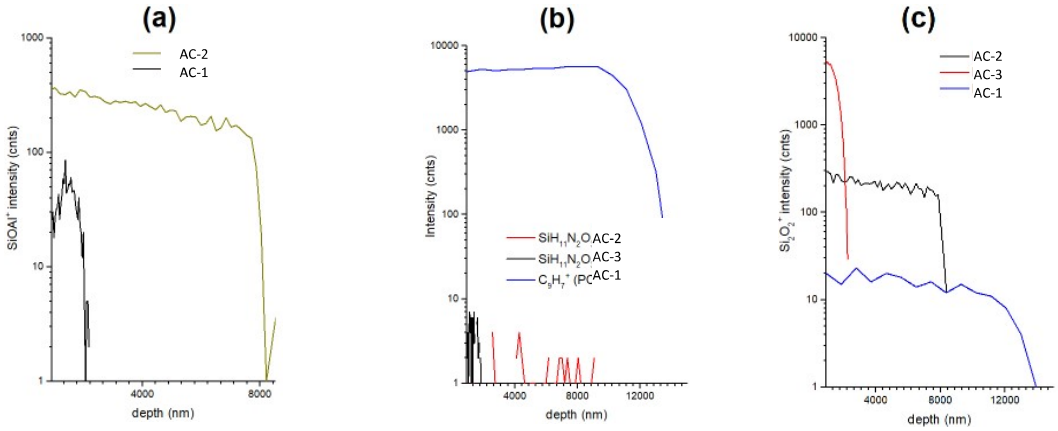

Figure 9. ToF-SIMS depth profile (positive ion mode) where (a) $AlOSi^+$ is drawn for AC-2 and AC-3; (b) $SiH_{11}N_2O_3^+$ is drawn for AC-2 and AC-3 and $C_9H_7^+$ for AC-1 and (c) $Si_2O_2^+$ is drawn for AC-2, AC-3 and AC-1.

The effect of the physical barrier by a high film thickness cannot be supported by ToF-SIMS analysis. However, it should be noted that the physical barrier caused by the high coating thickness in AC-1 does play a significant role in the corrosion resistance. The results show AC-1 acts more as an organic coating rather than a coating as in the case of AC-2 and AC-3 notably.

The contributions to corrosion resistance of the 3 samples can be classified as follows. The occurrence of interface bond was found for the 3 coatings with significant differences. In the case of AC-1, the detection of the corresponding $AlOSi^+$ fragment could only be performed by a long acquisition around the coating/ Al substrate interface. In contrary, AC-2 and AC-3 revealed direct detection in the profiles, while AC-3 displayed a more localized $AlOSi^+$ fragment around the interface than AC-2.

The second important feature concerns the barrier properties revealed by the $Si_2O_2^+$ fragment with the highest relative intensity for AC-3, a relatively lower intensity for AC-2 and a minimal intensity for AC-1. In the case of AC-1, the high relative intensity of $C_9H_7^+$ reveals the presence of an organic coating that may contribute significantly to the barrier properties.

While examining the two first important features for corrosion resistance, it turned out that AC-3 and AC-1 can both be qualified as “” coatings, due to occurrence of $SiOAl^+$ over an extended depth (several hundreds of nm and several micrometers, respectively). That is however not the case for AC-1, due to the fact that $SiOAl^+$ cannot be directly detected.

As far as the coating thickness parameter is concerned, its precise contribution cannot be properly discussed, given that the thicknesses measured for the 3 samples are very different. However, several points can be made at this stage. Firstly, the coating thickness was measured (Figure 4) as maximum for AC-1 (17.65 µm), whereas it is minimum in the case of AC-3 (2.3 µm), and intermediate in the case of AC-2 (9.75 µm). As the best corrosion resistance is attributed to AC-3, we can deduce that the coating thickness parameter is not the most important, compared to interface bonding and cross-linking of the coating. However, this parameter cannot be considered negligible, as it has been shown to improve the properties of AC-1 compared with AC-2.

4. Conclusions

In this work, we studied the corrosion resistance of 3 different silicon-based coatings on an aluminum 2024 substrate by salt spray testing, and in addition, by ToF-SIMS analysis. As an important finding we could, in part, correlate the salt spray test results with in-depth ToF-SIMS profiles made with a GCIB source that allows the molecular character of all peaks to be preserved. We could in fact relate to the main chemical factors contributing to high corrosion resistance, which are of the aluminum surface to inert $AlOSi^+$ and the formation of $Si_2O_2^+$ indicative for the crosslink density and responsible for the barrier properties with the ToF-SIMS analysis. AC-3 showed strong peaks of $AlOSi^+$ and $Si_2O_2^+$ and consequently showed the highest corrosion resistance. AC-2 showed lower intensity peaks for both $AlOSi^+$ and $Si_2O_2^+$ and subsequently performed worse in the salt spray tests. In the case of AC-1, we hardly detect $AlOSi^+$ and $Si_2O_2^+$ moieties but we noted the presence of an organic fragment throughout the coating (cf. $C_9H_7^+$), which may help to improve the properties of AC-1 over those of AC-2. Moreover at 16.5 µm, the layer thickness of AC-1 was most profound which likely supports the anticorrosion properties as known from organic coatings. The detection of interface bonding was found to be a highly significant factor in corrosion resistance, not only in the detection of the corresponding fragments ($SiOAl^+$), but also in specific location within the overall layered structure. Beyond being qualified as “” coating, AC-3 was found to have the best values for both characteristics.

As this work establishes a good correlation between salt spray tests and ToF-SIMS results for a set of three anticorrosion coatings, it may pave the way for the expansion of a correlation database, and ultimately discriminate corrosion resistance on the basis of ToF-SIMS results instead of the usually employed and costly salt spray tests.

CONFLICT OF INTEREST

The authors declare no conflict of interest.

DATA AVAILABILITY STATEMENT

The data that support the findings of this study are available from the corresponding author upon reasonable request.

REFERENCES

(1) European Chemicals Agency *Understanding REACH [Online]. Available, https://echa.europa.eu/regulations/reach/understanding-reach*.
(2) De Graeve, I.; Vereecken, J.; Franquet, A.; Van Schaftinghen, T.; Terryn, H. *Progress in Organic Coatings* **2007**, *59*, 224.
(3) Franquet, A.; Van Schaftinghen, T.; Terryn, H.; Subramanian, V.; Van Ooij, W. *ATB-Metallurgy* **2000**, 207.
(4) Jonschker, G. *Sol-Gel-Technology in Praxis*; Vincentz Network, 2014.
(5) Wang, D.; Bierwagen, G. P. *Progress in Organic Coatings* **2009**, *64*, 327.
(6) WO2010/095146A1 *Anti-corrosion sol-gel hybrid coating on zinc and zinc alloy steel sheets and preparing method thereof.*
(7) US 6, 060 *Sol for bonding epoxies to aluminum or titanium alloys.*
(8) Benninghoven, A.; Rüdenauer, F. G.; Werner, H. W. *Secondary Ion Mass Spectrometry: Basic Concepts, Instrumental Aspects, Applications, and Trends*; J. Wiley, 1987.
(9) Abel, M. L.; Digby, R. P.; Fletcher, I. W.; Watts, J. F. *Surface and Interface Analysis* **2000**, *29*, 115.
(10) Marcoen, K.; Gauvin, M. l.; De Strycker, J.; Terryn, H.; Hauffman, T. *ACS omega* **2020**, *5*, 692.
(11) Abel, M.-L.; Rattana, A.; Watts, J. F. *Langmuir* **2000**, *16*, 6510.
(12) Marcoen, K.; Gauvin, M.; De Strycker, J.; Terryn, H.; Hauffman, T. *The Journal of Physical Chemistry C* **2020**, *124*, 13150.
(13) Gharbi, O.; Thomas, S.; Smith, C.; Birbilis, N. *npj Materials Degradation* **2018**, *2*, 12.
(14) Castle, J. *The Journal of Adhesion* **2008**, *84*, 368.
(15) Hu, J.-M.; Ji, W.-G.; Liu, L.; Zhang, J.-Q.; Cao, C.-N. *Silanes and other coupling agents* **2009**, *5*, 203.